Alinejad, Farid; Bordbar, Hadi; Hostikka, Simo

Development of full spectrum correlated k-model for spectral radiation penetration within liquid fuels

1 **Development of Full Spectrum Correlated k-Model for Spectral Radiation Penetration**
2 **Within Liquid Fuels[1]**

3 **Farid Alinejad[1], Hadi Bordbar[1*], Simo Hostikka[1]**

4 **[1]**Department of Civil Engineering, Aalto University, Finland

5 Abstract

6 In this paper, the full spectrum correlated k-distribution (FSCK) models are developed for several liquid fuels
7 including decane, ethanol, ethylene glycol, heptane, and toluene. The models were built using high-resolution
8 absorption spectra, collected from the literature. To validate the novel FSCK models, they were used to solve radiative
9 heat transfer within liquid pools assuming three temperature profiles (i.e. constant temperature, linear and nonlinear
10 temperature profiles) and the calculated transmissivity and radiative heat source of FSCK were compared with those
11 of using high resolution absorption spectra and the gray models implementing the Planck mean absorption coefficient.
12 The sensitivity analysis was performed for the accuracy of the FSCK results with number of quadrature points for
13 different fuels. Using seven quadrature points for FSCK model has been found to be sufficient for providing good
14 accuracy of spectral radiative heat transfer within the liquid fuels with a reasonable computational cost. Moreover, we
15 studied the effect of the reference temperature used in FSCK model and found out that for the pool fire scenario, the
16 FSCK provides its best accuracy if an equivalent temperature representing the radiation feedback from the flame is
17 used as the reference temperature. Comparison of computational costs of high-resolution spectral radiation
18 calculations and FSCK method revealed a significant computational gain by use of FSCK model.

19 **Keywords:** FSCK method, Spectral thermal radiation, radiation penetration in liquid fuels, reference temperature,
20 pool fire, transmissivity.

21 Nomenclature

Abbreviation		T	Temperature (K)
FSCK	Full-Spectrum Correlated K-distribution	n	Refractive index
LBL	Line-by-line	$\hat{n}$	Normal unit vector
QP	Quadrature Points	$\bar{n}$	Weighted average of refractive index
SLW	spectral-line based weighted-sum-of-gray-gases	n_λ	Spectral refractive index
WSGG	weighted sum of gray gases	$\dot{q}'''_{rad}$	Radiative heat source (W/m^3)

Latin

a	The ratio of any two full-spectrum k-distributions	$(\dot{q}''_\lambda)^+$	Forward spectral radiative heat flux (W/m²/m)
c_0	Velocity of light in vacuum (m/s)	$(\dot{q}''_\lambda)^-$	Backward spectral radiative heat flux (W/m²/m)
f	Full-spectrum k-distribution (m)	V	Volume of liquid medium (m³)
g_i	Cumulative k-distribution for the ith quadrature point	w	Weighting parameter for Gauss-Chebyshev quadrature scheme
h	Planck's constant (m²kg/s)	x	Path length (m)
I	Total intensity (W/m²/sr)	**Greek**	
I_b	Blackbody total intensity (W/m²/sr)	ε_{eff}	Effective emissivity
I_{bw}	Wall blackbody total intensity (W/m²/sr)	ε_{flame}	Flame emissivity
$I_{bw\lambda}$	Wall blackbody spectral intensity (W/m²/m/sr)	ε	Wall emittance
$I_{b\lambda}$	Blackbody spectral intensity (W/m²/m/sr)	κ_p	Planck-weighted radiation absorption coefficient (m⁻¹)
I_g^+	Forward radiation intensity in g space (W/m²/sr)	κ_λ	spectral absorption coefficient (m⁻¹)
I_g^-	Backward radiation intensity in g space (W/m²/sr)	λ	Wavelength (μm)
I_λ^+	Forward spectral intensity (W/m²/m/sr)	τ	Transmissivity
I_λ^-	Backward spectral intensity (W/m²/m/sr)	ϕ	State parameter
k	Absorption coefficient (m⁻¹)	**Subscripts**	
k^*	Correlated k value (m⁻¹)	in	input
k_B	Boltzmann constant (m²kg/s²/K)	out	output
k_r	Imaginary part of complex refractive index	ref	Reference
$\hat{s}$	Direction unit vector	wb	Bottom wall
		wu	Upper wall

22

1. Introduction

23

24   To calculate the radiative heat transfer in participating media, the radiative transfer equation

25   (RTE) must be solved. In contrast to other modes of heat transfer, radiative heat transfer is

26   dependent on the direction and wavelength of the radiation intensity, so extra treatment is needed

27   to account for directional and spectral dependency [1, 2]. Therefore, for a precise prediction of

28 radiative heat transfer inside participating media, the RTE must be solved for each fine enough

29 spectral interval using a constant absorption coefficient (i.e. line-by-line calculation) [3]. Spectral

30 absorption coefficient shows a complex change with wavelength that needs to be included in the

31 RTE solution. For doing this, diagram of spectral absorption coefficient must be divided into very

32 fine spectral intervals especially for molecular gases. Literature review of the gas spectral radiation

33 heat transfer modeling suggests that a $d\eta < 0.02$ to be used for the line-by-line (LBL) calculation

34 in gaseous media. Doing such a calculation coupled with other transport equations is

35 computationally very demanding. Therefore, LBL is applied only for the setting benchmarks,

36 developing of the radiation models, and validating of one-dimensional problem [3, 4, 5]. In liquid

37 media, the changes of the spectral absorption coefficient are smoother than those of gases,

38 therefore a wider spectral interval can be used for the integration. In this paper, we use the term of

39 high-resolution method for using the finest available spectral absorption data of liquid fuels for

40 solving spectral RTE. This method is analogous to the LBL calculations used in the literature of

41 gas spectral radiation heat transfer modeling.

42   Several simplified models have been proposed to account for the non-gray radiative heat

43 transfer for gas phase. The most common models are the banded approaches [6, 7], weighted sum

44 of gray gases model (WSGG) [8, 9], the spectral-line based weighted sum of gray gases [10, 11],

45 and the full spectrum k-distribution (FSK) method [12, 13]. While banded models provide a gray

46 absorption coefficient for limited spectral intervals, i.e. gray bands, and therefore can provide

47 spectral information of radiative heat transfer in different bands, the global models such as WSGG,

48 SLW and FSK methods aim at providing accurate total values of thermal radiation. In the FSK

49 method, wavelengths of the absorption spectrum for the homogenous medium are reordered and a

50 monotonic increasing function of the reordered wavelength is obtained which allows each

51 absorption coefficient to be considered only once in the RTE calculations [14]. To support

52 inhomogeneous media, the FSK method is extended and different modified versions such as full-

53 spectrum correlated-k distribution method (FSCK) have been developed. This method assumes

54 that the spectral absorption coefficient of a participating medium at a local thermal state can be

55 correlated with the absorption spectrum of a reference state [15]. The accuracy of this method

56 therefore depends on the validity of this assumption; however, it allows modeling of various

57 combustion domains without having the detailed values of the absorption coefficient at different

58 thermal states [16, 17]. Furthermore, using look-up tables [18, 13, 19] to obtain the FSCK model

59 parameters made the method computationally efficient for different thermal radiation problems

60 [18]. These look-up tables have been reported in the literature for the most important gas species

61 found in combustion systems.

62   The next step in the development of global models is to extend them to support the radiation

63 transfer within multiphase flows. Although the spectral thermal radiation of the particulate phase

64 (e.g. solid particles and droplets) has been shown to be important in combustion applications [13,

65 20, 21], solving RTE for particles is mostly done by gray medium assumption [22, 23]. In one of

66 the first attempts to use the global models in solving the thermal radiation within the multiphase

67 flows, Wang et. al. [13] applied the FSK method for both gas-soot mixture and particles to

68 calculate the accurate radiation contribution of soot particles and improve the look-up table data

69 for FSCK parameters of gas-particle mixtures. They showed that the use of the coupled FSK-FSK

70 method for gas-soot-particle mixtures in 1D slab benchmarks significantly improves the results

71 compared to those of obtained through the coupled FSK-Gray method. Their developed FSK-FSK

72 method is based on an assumption that the absorption coefficient of the gas-soot mixture at a

73 reference thermodynamic state ϕ_0 can be correlated with the absorption coefficients of both gas-

74 soot mixture and particles at their local thermodynamic state ϕ_i. However, this assumption might

75 be violated in practical conditions especially in gas-liquid systems where the droplets or fuel pools

76 are at a very different temperature compared to the the gas-soot temperature.

77 An application in which the radiation transport within a condensed phase has a substantial effect

78 is liquid pool fires. The experimental investigations of Hamins and coworkers [24] showed that

79 thermal radiation comprises about 80 and 96 percent of the heat feedback for a 0.3 m heptane and

80 toluene pool fires, respectively. The liquid fuel evaporation rate plays a significant role on the

81 evolution of fires, ignition time and their heat release rate [25]. Evaporation rate is governed by

82 the radiative heat feedback from the flame and the convective and conductive heat flows within

83 the gases above the liquid surface as well as in the liquid phase itself [26]. Therefore, without

84 accurate modeling of these heat transfer mechanisms in the liquid domain, accurate prediction of

85 the evaporation rate is not feasible. Besides the experimental investigations for the radiative heat

86 flux from flame zone and its penetration through liquid fuels [27, 28], most of the numerical studies

87 in this field have used gray models, in which a mean absorption coefficient is used to solve the

88 RTE [29]. For gray modeling, either Planck-mean absorption coefficient or an effective absorption

89   coefficient calculated by measured data of transmissivity at a depth of the liquid and assuming an

90   effective length were used in the previous research [21, 29]. The results of the present paper will

91   show that error in prediction of radiative heat source with the former one is quite remarkable, even

92   close to 100% in some cases. The latter method, i.e. using an effective mean absorption coefficient

93   has also been found inaccurate [30] as it filters most of the spectral absorption features of liquids

94   occurring in the very first layers. Moreover, it needs a guess for mean path length which is a kind

95   of black art. In one of the only spectrally resolved numerical works in this field [30], the

96   transmittance through liquid heptane was calculated by using the k-distribution method. In that

97   research, it was assumed that the temperature gradient within liquid fuel does not have a significant

98   effect on transmission, therefore the k-distribution method for a medium with a constant

99   temperature was applied. It was concluded that using of k-distribution method (k-D) improves the

100   accuracy of calculations compared to using an equivalent gray absorption coefficient. Furthermore,

101   the great privilege of k-D method for the computational cost compared to high-resolution

102   integration method was reported. In that work, by ignoring the change of temperature within the

103   liquid pool, the emission of liquid was neglected and a simplified RTE was solved. It is a valid

104   simplification in many cases where the temperature of radiation source, e.g. fire flame, is high.

105   However, for the situations with low values of radiation intensity reaching the fuel surface in the

106   pools, such as having low view factors, the emission of liquids would be more important and

107   therefore cannot be ignored. This formed the motivation for the present research, along with the

108   need to extend the modelling to other fuels than heptane and provide the tabulated data for their

109   FSCK model parameters.

110   To complete the previous work [30], in this paper, we develop a full spectrum correlated k-

111   distribution (FSCK) models for spectral radiative heat transfer in five heavy hydrocarbon liquid

112   fuels. To validate the presented model, it is used to solve the radiation penetration within the liquid

113   pools with various temperature distributions. Three different temperature profiles are considered

114   for the liquid including a homogenous constant room temperature and two inhomogeneous

115   temperature profiles. The accuracy of the FSCK models are verified by comparing its predictions

116   with those of using high-resolution spectral absorption coefficient in solving the spectral RTE.

117   Hence, this paper advances our previous research [30] and extends it to more general conditions

118   with considering the effect of liquid emission and solving the complete RTE.

5

2. Theory

As the main scope of the present research is to develop and validate the FSCK models for liquid fuels, the radiation flux reaching from the flame to the pool is simplified to be perpendicular to the liquid interface. By this, the radiation penetration within the liquid is solved with a simple two flux method. Nevertheless, the developed FSCK model is readily usable by other more complex RTE solvers such as discrete ordinate (DO) or P-1 approximation methods. For the sake of completeness, the theory of two flux RTE solver is briefly presented in the following section. It is followed by a short description of the FSCK method.

2.1. Solution method for spectral radiative transfer equation in a liquid pool

To solve thermal radiation in a pool fire scenario, the spectral RTE for absorbing, emitting and non-scattering liquid can be solved by two-flux method [31]. The directionally integrated intensity over a hemisphere along the incoming radiation (I_λ^+) can be solved with the following equation:

$$\frac{1}{2}\frac{dI_\lambda^+}{ds} = \kappa_\lambda(I_{b\lambda}(T) - I_\lambda^+) \tag{1}$$

where κ_λ and $I_{b\lambda}$ represent the spectral absorption coefficient and the spectral blackbody intensity at medium temperature of T, respectively. Assuming that the radiation reaching the liquid surface can be simplified to radiation of a gray wall, the boundary condition for the equation (1) is given as:

$$I_{\lambda,w}^+ = \varepsilon_{wu}I_{bw\lambda} + (1 - \varepsilon_{wu})I_{\lambda,w}^- \tag{2}$$

where, ε_{wu} and $I_{bw\lambda}$ show the emissivity and blackbody spectral intensity of the upper wall, respectively.

Equations (1) and (2) consider detailed spectral distribution for radiation transport within the medium. Integrating the spectral intensity over the entire spectrum, gives the total intensity is the results of this so-called high-resolution integration method will be used as a reference solution to estimate the accuracy of other simplified models considered to account for spectral absorption of medium. Transmissivity is then calculated by

$$\tau = \frac{I_{out}^+}{I_{in}^+} \tag{3}$$

142 where, parameters I_{in}^+ and I_{out}^+ show the total incident intensity at the boundary and the forward

143 intensity at any depths within the liquid fuel. Radiative heat source as a function of depth is

144 calculated as:

$$\dot{q}'''_{rad,\lambda} = \frac{d(\dot{q}''_\lambda)^+}{dx} + \frac{d(\dot{q}''_\lambda)^-}{dx} \tag{4}$$

145 where $(\dot{q}''_\lambda)^+ = \pi I_\lambda^+$ and $(\dot{q}''_\lambda)^- = \pi I_\lambda^-$. Finally, the total radiative heat source is estimated by

146 integrating over the entire spectrum:

$$\dot{q}'''_{rad} = \int_0^\infty \dot{q}'''_{rad,\lambda} d\lambda \tag{5}$$

147 **2.2. Full-spectrum correlated k-distribution (FSCK) method**

148 One of the most well-known global methods to solve non-gray RTE, is the full-spectrum-

149 correlated k-distribution (FSCK) method. This method is based on reordering wavelength in order

150 to transform the complex absorption spectra to a monotonically increasing function of a reorder

151 wavelength. The details of this method are well documented in several references including [16,

152 14]. Here, for the sake of completeness, it is briefly reviewed. In the global model, the integrated

153 form of the spectral RTE is solved. For FSCK, a full spectrum k-distribution is defined as:

$$f(T, \phi, k) = \frac{1}{I_b} \int_0^\infty I_{b\lambda}(T) \delta(k - \kappa_\lambda(\lambda, \phi)) d\lambda \tag{6}$$

154 where δ is the Dirac delta function. The function $f(T, \phi, k)$ determines the weight of each k value

155 in the assumed k-distribution using the high-resolution spectral absorption coefficient (κ_λ). To

156 extend the method for inhomogeneous gaseous media [16] , a reference state (e.g. temperature,

157 pressure, and concentration of gas species in gaseous media) have to be considered in equation (6),

158 because the spectral absorption coefficient of molecular gases strongly changing with their thermal

159 states. Here, for liquid fuels, a literature survey shows that the change of spectral absorption

160 coefficient of heavy hydrocarbon liquid fuels with temperature is negligible. For instance, the

161 experimental studies of Wang et. al. [32] and Ai et. al. [33] showed a negligible change of spectral

162 absorption coefficient with temperature for liquid fuels such as isopropanol, n-butanol, n-decane,

7

163   diesel, gasoline, and jet fuel. Hence, the change of spectral absorption of liquid fuels with

164   temperature is assumed negligible and ignored in development of the FSCK model in the present

165   work.

166   Integrating of equation (1) over the entire spectrum of thermal radiation, the following

167   equation is obtained:

$$\frac{1}{2}\frac{dI_k^+}{ds} = k(f(T,k)I_b - I_k^+) \tag{7}$$

168   where, I_k^+ is defined as:

$$I_k^+ = \int_0^\infty I_\lambda \delta(k - \kappa_\lambda) d\lambda \tag{8}$$

169   For the boundary condition, the same integration is done for equation (2) and gives:

$$I_k^+ = \varepsilon_{wu} f(T_w, k) I_{bw} + (1 - \varepsilon_{wu}) I_k^- \tag{9}$$

170   In equation (7), $f(T,k)$ approaches infinity in the extremum points of the spectral absorption

171   coefficient profiles. To overcome with this issue, the new spectral variable $g(T,k)$ is introduced

172   as the cumulative integral of $f(T,k)$ as:

$$g(T,k) = \int_0^k f(T,k) dk \tag{10}$$

173   This parameter exhibits a monotonically increasing changes with respect to k values and therefore

174   can be approximated by a limited number of discrete points. The cumulative k-distribution

175   function (g) varies between zero and one and in some references is called reordered wavelength

176   [34, 35]. Integrating equation (7) over the entire k domain gives the following equation:

$$\frac{1}{2}\frac{dI_g^+}{ds} = k(T_{ref}, g_{ref})\big(a(T, T_{ref}, g_{ref})I_b - I_g^+\big) \tag{11}$$

177   where T_{ref} is known as the reference temperature which has to be selected.

178   Note that Eq. (11) is the earliest form of RTE developed for FSCK method by Modest [14]. This

179   form does not preserve the emission well and therefore introduces some inaccuracy for the cases

180   where emission is dominant such as hot combustion gases. To overcome with this drawback, Cai

181   and Modest [36] presented a newer formulation for FSCK which well preserves the emission by

182   using the correlated-k obtained by the absorption spectrum of the local state and using the local

183   temperature as the Planck temperature. For liquid fuels in this study, the problem is not emission

184   dominated and the accuracy of results mainly dependent on the absorption of the liquid. We will

185   show later that this original form of FSCK well serves the emission of liquid fuels and therefore

186   this original form is good enough to be used.

187   For the boundary condition, the following equation is attained:

$$I_g^+ = \varepsilon_{wu} a(T_w, T_{ref}, g_{ref}) I_{bw} + (1 - \varepsilon_{wu}) I_g^- \tag{12}$$

188   where I_g^+ is defined as:

$$I_g^+ = \int_0^\infty I_\lambda \delta(k - \kappa_\lambda(\lambda)) d\lambda / f(T_{ref}, k) \tag{13}$$

189   To abstract the equations (11) and (12), the parameter $a(T, T_{ref}, g_{ref})$ is defined as:

$$a(T, T_{ref}, g_{ref}) = \frac{f(T, k)}{f(T_{ref}, k)} = \frac{dg(T, k)}{dg_{ref}(T_{ref}, k)} \tag{14}$$

190   Several options to select the reference temperature for applying FSCK model in gaseous

191   combustion systems have been proposed such as maximum or minimum temperature of the

192   computational domain, volume averaged temperature, and emission weighted temperature [16].

193   References [16, 17] showed that using volume average of the fourth-power of temperature,

$$T_{ref}^4 = \frac{1}{V} \int_V T^4 \, dV \tag{15}$$

194   and Planck-mean temperature,

$$(\kappa_p T^4)_{ref} = \frac{1}{V} \int_V \kappa_p T^4 \, dV \tag{16}$$

9

195   are appropriate to use as the reference temperature in gaseous media. In the next sections of this
196   paper, the effect of using different reference temperatures in solving spectral radiation with FSCK
197   model in liquids will be investigated.

198   After obtaining I_g^+, the total forward intensity is calculated as:

$$I^+ = \int_0^1 I_g^+ \, dg \tag{17}$$

199   Deriving the FSCK equations for the backward radiation intensity is done in the similar way. For
200   solving the FSCK equations and get the radiative heat source, the Gauss-Chebyshev method has
201   been applied as explain in [37].

2.3. Gray model

203   One of the common approximations to account for the spectral variation of absorption
204   coefficient of participating media in calculations of radiative heat transfer is using only one average
205   absorption coefficient for the entire thermal radiation spectrum and solve the RTE only once with
206   that so-called gray absorption coefficient. Due to its simplicity and low computational cost, this
207   model has been widely used in engineering calculations especially for the particulate phase.
208   Several ways have been proposed to calculate the gray absorption coefficient from which using
209   the Planck mean absorption coefficient is most popular. In this method, Planck intensity is used as
210   the weighting factor for averaging the spectral absorption coefficient over the spectrum:

$$\kappa_p = \frac{\int_0^\infty I_{b\lambda}(T)\kappa(\lambda)d\lambda}{\int_0^\infty I_{b\lambda}(T)d\lambda} \tag{18}$$

211   Therefore, κ_p is the function of local temperature of medium.

212   To exhibit the advantage of developed FSCK model, we included the gray modeling with the
213   Planck mean absorption coefficients in the case studies of the present paper. The Planck mean
214   absorption coefficient used in gray calculations is calculated either by using the local temperature
215   of the liquids or an equivalent temperature of incident radiation at the boundary.

2.4. Boundary conditions

217   For the sake of model development, we assume a black wall ($\varepsilon_{wu} = 1$) at certain temperature

218   to represent the thermal condition of the upper surface of the liquid pool. With this assumption, by

219   following Eq. (2) the boundary condition for the high-resolution spectral RTE solution is given as:

$$I_\lambda^+ = I_{bw\lambda} \tag{19}$$

220   For the backward radiation, the boundary condition at the bottom of the liquid layer by assuming

221   a gray wall is given as:

$$I_\lambda^- = \varepsilon_{wb} I_{bw\lambda} + (1 - \varepsilon_{wb}) I_\lambda^+ \tag{20}$$

222   where the parameter ε_{wb} is the wall emissivity. Here, in order to make the problem similar to real

223   pool fires and enter the effect of reflection from pan's bottom wall, we assumed the wall emissivity

224   to be 0.5. Nevertheless, due to the small temperature of bottom wall compared to the radiation

225   from the flame, the bottom wall emittance has evidently a negligible effect on the results of our

226   test cases.

227   In the case of FSCK method, the boundary condition for the forward radiation with assuming black

228   wall for upper surface is given as:

$$I_g^+ = I_{bw} \tag{21}$$

229   For the backward radiation, the following equation has been applied as boundary condition for the

230   gray bottom wall:

$$I_g^- = \varepsilon_{wu} a(T_w, T_{ref}, g_{ref}) I_{bw} + (1 - \varepsilon_{wu}) I_g^+ \tag{22}$$

231   For the gray method, the boundary conditions for RTE in upper and lower walls have been applied

232   in form of equation (23) and (24) respectively:

$$I^+ = I_{bw} \tag{23}$$

$$I^- = \varepsilon_{wu} I_{bw} + (1 - \varepsilon_{wu}) I^+ \tag{24}$$

233   **2.5. Absorption spectra of the liquid fuels**

The data of spectral complex index of refraction needed for calculating the absorption coefficient of the considered liquid fuels, i.e. decane, ethanol, ethylene glycol, heptane, and toluene were extracted from different experimental papers in the literature. Summary of these references and their covered wavelength regions are shown in the Table 1.

Table 1- Summary of the experimental studies used for extracting the spectral complex index of refraction or the spectral absorption coefficient of the liquid fuels.

Fuel	Wavelength region (μm)	Reference
Decane	1.66-18.78	[32]
Ethanol	0.185-60.93	[38]
Ethylene glycol	0.19-29	[39]
Heptane	0.65 – 1.3	[40]
	1.3 – 2.0	[41]
	2.0 – 14.92	[42]
Toluene	0.5-1.75	[43]
	1.75-23	[44]

All the calculations for different radiation spectral models (i.e. high-resolution, FSCK, and gray model) were done for the spectral regions presented in Table 1. The spectral absorption coefficient of the liquids is calculated by using the imaginary part of the complex refractive index k_r as:

$$\kappa_\lambda = \frac{4\pi k_r}{\lambda}$$

(25)

The calculated absorption spectra of these five liquid fuels are shown in Figure 1.
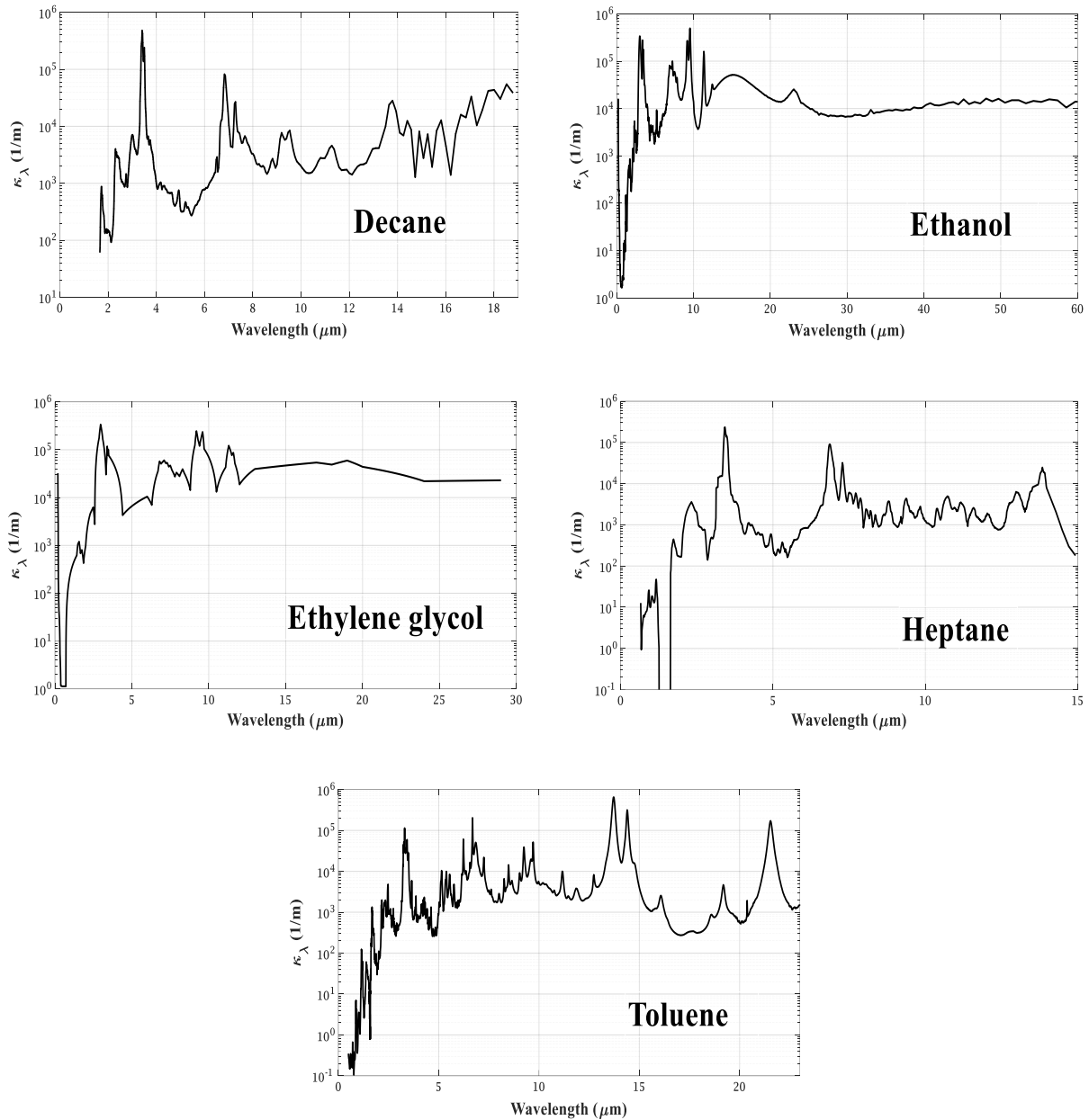
Figure 1- The calculated spectral absorption coefficient for decane, ethanol, heptane, ethylene glycol, and toluene.

In contrary to gaseous media, the real part of the complex index of refraction for these liquids is larger than unity and therefore should be included in calculation of emission term in RTE using the Planck intensity. In spectroscopic measurement of spectral complex index of refraction of liquids, the wavelength is set for air and the spectral absorption data are hence reported as a function of wavelength of the electromagnetic waves in air. Therefore, in calculation of emission within the liquids, the reported wavelengths must be modified applying the real part of complex index of refraction for each fuel.

13

258   The real part of the spectral complex index of refraction, i.e. also known as the refractive

259   index n_λ, is also a spectral quantity. Here we investigate the significance of considering the spectral

260   distribution for the real part of the spectral complex index of refraction for the studied liquid fuels.

261   Among the considered liquid fuels, the n_λ of ethylene glycol shows the largest variation with

262   wavelength, therefore this liquid has been selected for this investigation. Considering a constant

263   value of $\bar{n}$ for the n_λ over the entire spectrum, the spectral blackbody intensity is calculated by

264   [45]:

$$I_{b\lambda}(T,\lambda) = \frac{2\pi h c_0^2}{\pi \bar{n}^2 \lambda^5 \left[\exp\left(\frac{h c_0}{\bar{n}\lambda k_B T}\right) - 1\right]} \tag{26}$$

265   where $\bar{n}$ can be estimated as:

$$\bar{n} = \frac{\int_0^\infty n_\lambda d\lambda}{\int_0^\infty d\lambda} \tag{27}$$

266   Our calculations show that considering or ignoring the spectral variation for the real part of the

267   complex index of refraction introduces only less than 2% difference in total blackbody emission

268   power of the ethylene glycol. Hence, we simply used the mean value for real part of the refractive

269   index (Eq. 27) as reported in Table 2.

270   *Table 2- Mean refractive index for liquid fuels*

Liquid fuel	Mean refractive index ($\bar{n}$)
Decane	1.40
Ethanol	1.39
Ethylene glycol	1.45
Heptane	1.38
Toluene	1.48

271

272   Using the spectral data of the liquid fuels presented in this section, we obtained the parameters

273   of FSCK model and the Planck mean absorption coefficients needed for non-gray and gray

274   simulations of radiative heat transfer within the liquid fuels. The results provide the grounds to

275   select a suitable number of quadrature points and the reference temperature for FSCK model to

276 accurately solve spectral radiation penetration within the studied liquid fuels. The details of the
277 analysis and the tabulated parameters of FSCK model are presented in the next section.

278 **3. Validation test cases**

279   The geometry of the validation case is a layer of fuel with thickness of 8 mm bounded from its
280 upper side with a black wall. The bottom side is assumed to be a gray wall at 300 K with emittance
281 of 0.5. To make the considered problem closer to a real fire scenario, the temperature of the upper
282 black wall is assumed to be 1450 K which is experimentally found to be a good approximation to
283 represent real flame intensity of reaching the fuel surface of a large pool fire of these fuels [41].
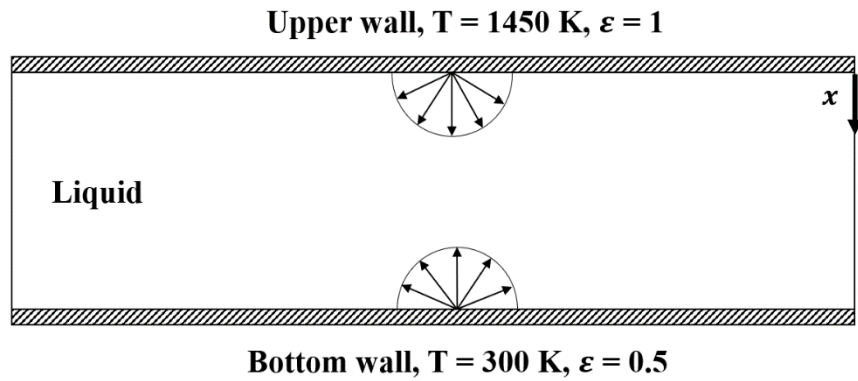284 The side walls are assumed to be far enough so that the radiation can be assumed one dimensional.

285

286 Figure 2 – Considered geometry in this paper

287   As a common practice to validate the spectral radiation models, they are applied to 1D
288 radiative transfer problem where the temperature profile is known and the radiation transfer is
289 decoupled from the other conservation equations [6, 8, 13]. We followed the same validation
290 strategy and assumed three different temperature profiles for the 1D liquid fuel layer:1) constant
291 temperature of 300 K, 2) linear profile between 300 K at the bottom and boiling temperature at the
292 surface, and 3) non-linear profile where the maximum temperature is just below the surface, which
293 has been experimentally observed in pool fires [46, 47]. The fuel-specific parameters of the
294 temperature profiles are presented in Table 3.

295

296

297

Table 3- the linear and nonlinear temperature profiles for liquid fuels in test cases 2 and 3.

Linear temperature profile: $\quad T(x) = ax + b$

Nonlinear temperature profile: $\quad T(x) = c.\exp\left(-\frac{d.(x-x_0)}{s}\right) - e.\exp\left(-\frac{f.(x-x_0)}{s}\right)$

Fuel	a	b	c	d	e	f	x_0	s
Decane	-18406.25	447.25	527.3	0.3538	92.41	1.269	0.00275	0.003594
Ethanol	-6440	351.52	348.3	0.104	0.7594	4.343	0.002938	0.003526
Ethylene glycol	-21343.75	470.75	865.3	0.5233	403.9	0.9174	0.002938	0.003526
Heptane	-8947.5	371.58	373.3	0.1519	6.496	2.5	0.002938	0.003526
Toluene	-10468.75	383.75	449.3	0.2466	69.75	1.055	0.002938	0.003526

299

300   The considered linear and nonlinear temperature profiles are shown in Figure 3.

301
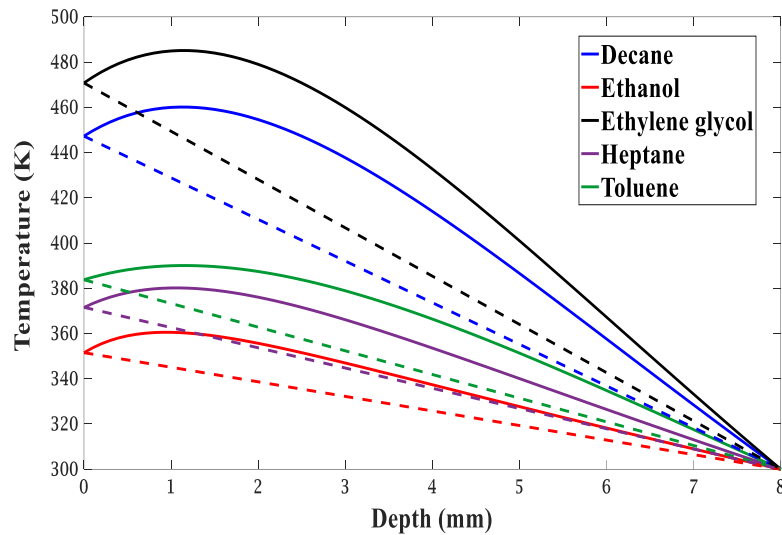
302

303   Figure 3- The considered temperature profiles for different liquid fuels; solid: Nonlinear profile and dash: Linear
304   profile.

305

Table 4- Different applied simulation cases for liquid fuels.

Case No.	Medium temperature profile	Boundary properties	
		$T_{source}\ (K)$	ε_{eff}
1	Constant	1450	1.0
2	Linear	1450	1.0
3	Nonlinear	1450	1.0
4	Constant	1450	0.04, 0.03, 0.01[*]
5	Linear	1450	0.04, 0.03, 0.01[*]
6	Nonlinear	1450	0.04, 0.03, 0.01[*]

[*] The effective emissivity of 0.04 and 0.03 has been applied for ethylene glycol and decane, respectively. For the rest of fuels, 0.01 is the value of effective emissivity.

Different combinations of the temperature profile, and effective emissivity are considered for six simulation cases, listed in Table 4. It is worth mentioning that the effective emissivity is considered to introduce different levels of incoming radiation to the liquid layer. It supports the sensitivity analysis to study the effect of emission of liquid as will be discussed in next sections. For the pool fire, the effective emissivity may represent the effect of emissivity of the flame, view factor of the pool in respect to the source of the radiation, and the deposition of soot on the liquid interface. Hence, the boundary condition for the FSCK models and gray calculations are given by Eq. (21) and (23), respectively in which I_{bw} is given as $\varepsilon_{eff} I_b(T_{source})$ or $\varepsilon_{eff} \sigma T^4$. For the benchmark solution using the high resolution spectral data, the boundary condition is given by Eq. (2) in which $\varepsilon_{wu} = 1$ and $I_{bw\lambda} = \varepsilon_{eff} I_{b,\lambda}(T_{source})$.

The boiling temperatures of heptane, ethanol, and toluene are 371.57, 351.53, and 383.75 K, respectively. Compared to decane and ethylene glycol with the boiling temperatures of 447.25 and 470.76 K respectively, these fuels have lower emission. In order to keep the incident intensity at the upper boundary and intensity by the liquid emission in the same order of magnitude, a lower value for the effective emissivity has been used for cases 4 to 6 as given in Table 4.

4. Results and discussion

All the presented results in this paper were calculated using 40 cells for 1D liquid domain. In order to check the mesh independency of the results, a simulation of radiation transfer inside the liquid heptane with using of 80, 60, and 40 grids have been conducted by using nonlinear

328 temperature profile for medium (case 3). Comparison of results shows that results by applying 40
329 grids are mesh independent as have been shown in Figure 4. For transmissivity and heat source
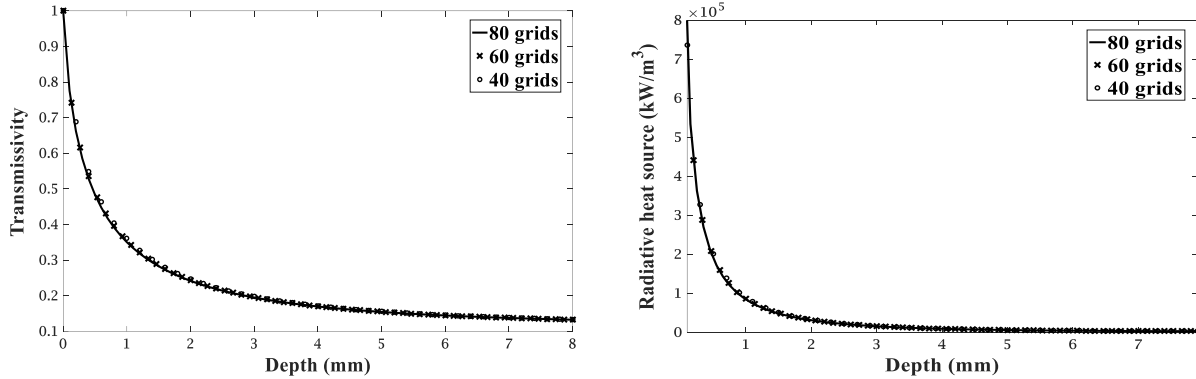330 results difference between 40 and 80 grids are near to 1 and 3 percent respectively.

331 Figure 4 – Calculated transmissivity (left plot) and radiative heat source (right plot) using 80, 60, and 40
332 computational grids for liquid heptane.

333   While the results of all introduced cases in Table 4 confirmed the privilege of FSCK model
334 compared to its counterpart of gray model, for the sake of brevity, among the first three cases, only
335 the figures of the third case with non-linear temperature profile are presented. To validate the
336 obtained FSCK model of different fuels and to address its accuracy, the results of FSCK model
337 and gray model are compared to those of high-resolution integration method. All FSCK
338 simulations have been done with up to 32 quadrature points (QP), therefore results have been
339 presented for the maximum number of quadrature points (i.e. 32) and 7 QP as an optimal choice.
340 The selection of 7 QP will be discussed later in this section.

341   In liquid fuels, a substantial part of the incident radiation is absorbed within a very thin
342 layer near the surface. Therefore, it is important for an appropriate radiative model to provide
343 accurate results in this region. To check this for the developed models of the present research, a
344 subplot of changes of radiative source term in this high absorbing region is included in the figures.

345   Figure 5 shows the results of high-resolution, FSCK, and gray models for heptane. For
346 FSCK model, using 32 QP exhibits an excellent agreement with the predictions of high-resolution
347 solution for both transmissivity and radiative heat source, although for the 7 QP results show
348 slightly lower accuracy. With increasing equivalent temperature of the incident intensity to the
349 liquid pool's interface, the peak region of the source intensity on the upper boundary shifts toward
350 left in wavelengths where the spectral absorption coefficient shows large fluctuations for heptane

351   and therefore more quadrature points are needed to accurately model the effect of all the k values.

352   However, for the lower temperature of the upper wall, high accurate predictions can be anticipated

353   by FSCK model even with quadrature points less than 7.
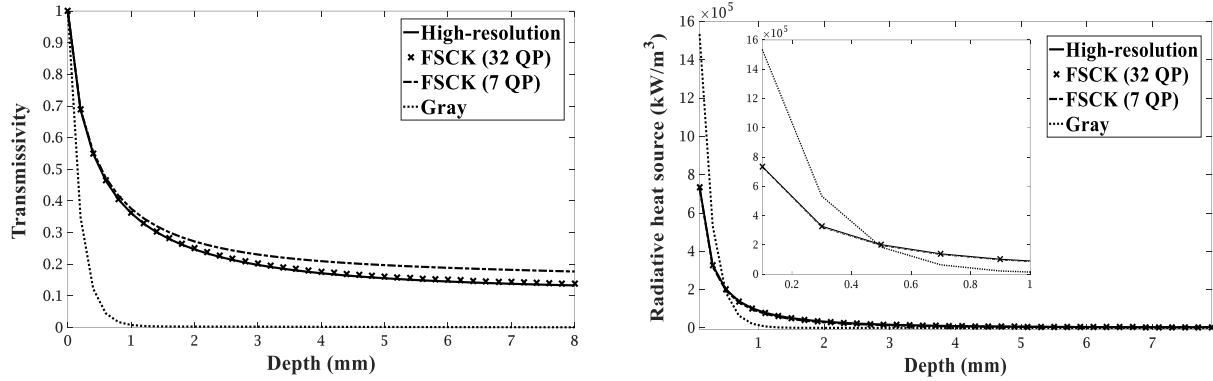

354   Figure 5 – Results of radiation transfer modelling within liquid heptane using different methods for transmissivity
355   (left) and radiative heat source (right).

356   Similar results have been presented for toluene in Figure 6. In this case, the comparison of

357   transmissivity and heat source for FSCK method with results of high-resolution method shows

358   very good agreement for 32 and 7 QP. For toluene, as shown in Figure 13, increasing the number

359   of quadrature points to 7 reduces the relative error to 3 %, a very good accuracy in prediction of
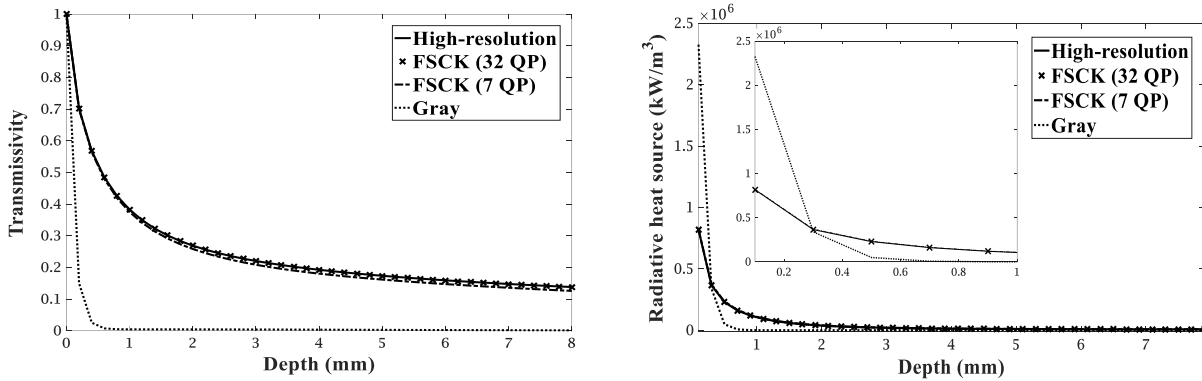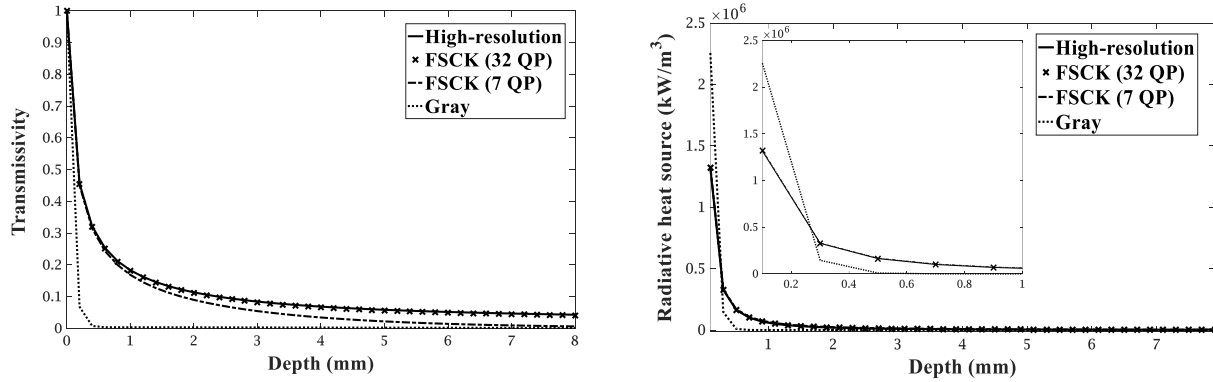
360   radiative heat source.

361   Figure 6 - Results of radiation transfer modelling within liquid toluene using different methods for transmissivity
362   (left) and radiative heat source (right).

363   The results of transmissivity and heat source for ethanol have been shown in Figure 7. Due

364   to high spectral absorption coefficient of ethanol, about 80 % of incident radiation has been

19

365 absorbed in thickness less than 1 mm from the liquid surface and only 10 % of the radiation

366 penetrates beyond 3 mm.

367 Figure 7 - Results of radiation transfer modelling within liquid ethanol using different methods for transmissivity
368 (left) and radiative heat source (right).

369 For decane, the calculated transmissivity and heat source are shown in Figure 8. In this

370 case, the average relative errors for FSCK method with 32 QP are near to 2 and 1 percent for

371 transmissivity and heat source, respectively. Similar to toluene, using 7 QP shows very good

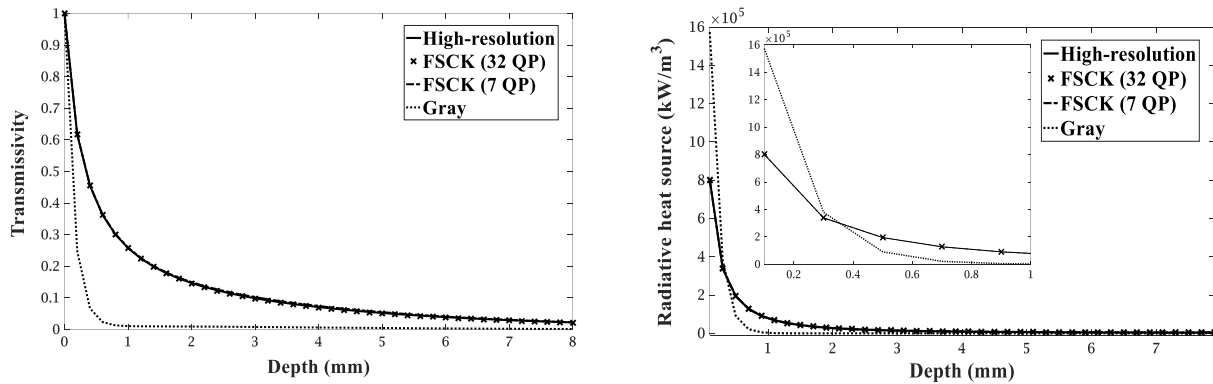372 agreement with results of high-resolution method as reported in Table 5.

373 Figure 8 – Results of radiation transfer modelling within liquid decane using different methods for transmissivity
374 (left) and radiative heat source (right).

375 Finally, simulation results of transmissivity and heat source for ethylene glycol have been

376 presented in Figure 9 . The relative errors of the calculated transmissivity and radiative heat source

377 for ethylene glycol for FSCK model with 32 and 7 QP is relatively higher than the previous cases.

378 As shown in Figure 13, increasing the number of quadrature points even up to 10, does not improve
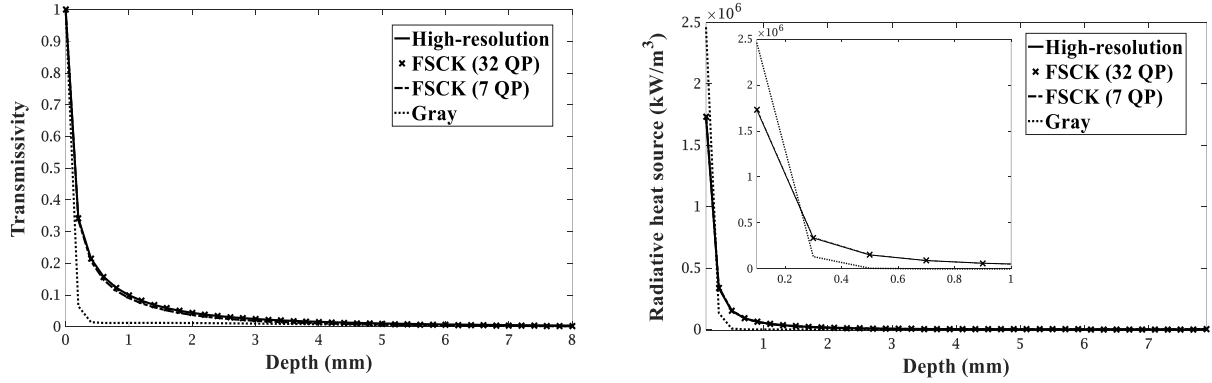
379 the accuracy reasonably.

20

Figure 9 - Results of radiation transfer modelling within liquid ethylene glycol using different methods for
transmissivity (left) and radiative heat source (right).

382   The poor accuracy in ethylene glycol can be attributed from two possible scenarios as (1)

383   not preserving the emission in FSCK and (2) inaccuracy of predicting absorption. To show the

384   accuracy of estimated emission term, the boundary condition has been set to zero to remove the

385   effect of the absorption of the incident intensity. Figure 10 shows the incident intensity at different

386   depths within a layer of ethylene glycol with different temperature profiles. It is seen that there is

387   a good agreement between results of high-resolution spectral calculation of emission and those of

388   the FSCK method with an average relative error less than 1%. Hence, the proposed FSCK model

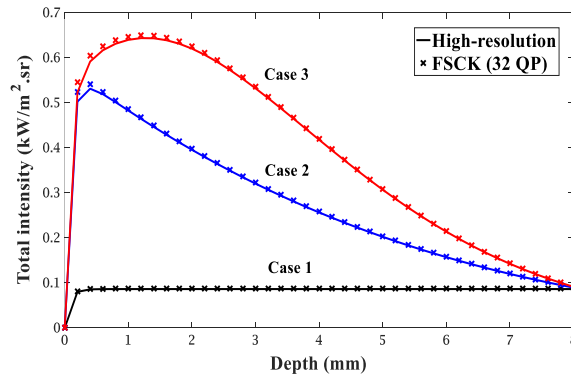389   well preserves the emission of the medium.

390

391   Figure 10- Comparison of calculated liquid emission for high-resolution and FSCK methods.

392   To investigate the second possible reason of poor accuracy in ethylene glycol, the profiles

393   of spectral intensity in a 1 mm layer of the ethylene glycol have been presented in Figure 11. To

394   calculate the k-distribution, the blackbody intensity at 1450 K has been used as the reference state.

395   Due to strong absorption of the ethylene glycol, a significant share of the intensity of the boundary

396   is absorbed within a 1 mm thickness of the liquid. Therefore, as shown in Figure 11, the shape of

21

397   intensity curve varies even by passing into very thin layer of liquid and misses the nature of the
398   blackbody intensity curve used as the reference state. It violates the main assumption of correlating
399   absorption in FSCK method, therefore, relatively large errors are observed for absorption term in
400   RTE. The same is also valid in ethanol within which the intensity curve undergoes the mentioned
401   change as shown in Figure 11.
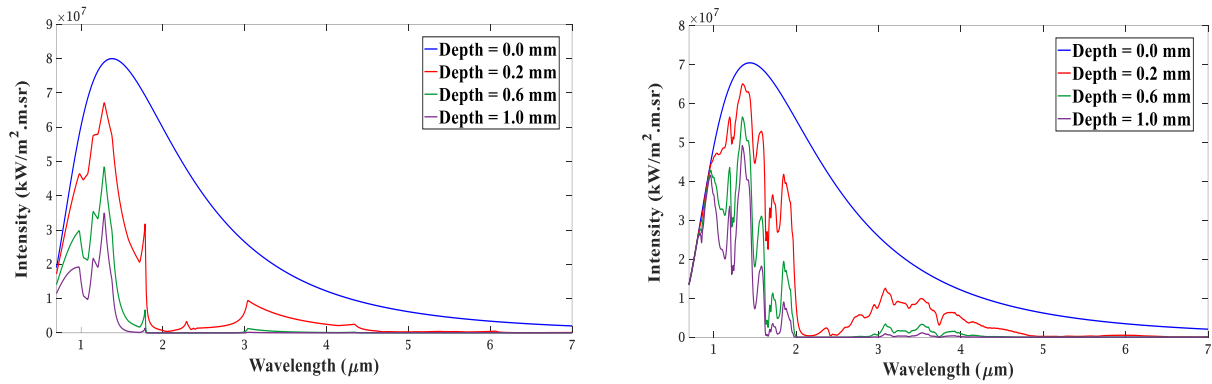

402   Figure 11- The calculated spectral intensity at different depths for case 1: up-left) ethylene glycol up-right) ethanol.

403   To further investigate this scenario, the profiles of spectral intensity for decane, toluene,
404   and heptane, for which the overall accuracy of the present FSCK method is better than ethylene
405   glycol and ethanol, have been shown in Figure 12. As seen in this figure, for decane, toluene and
406   heptane the shape of intensity curves is less deviated from the blackbody intensity curve used as
407   the reference state in the FSCK method. This observation is in line with the more accurate
408   transmissivity and source term of these two liquids compared to ethylene glycol and ethanol in
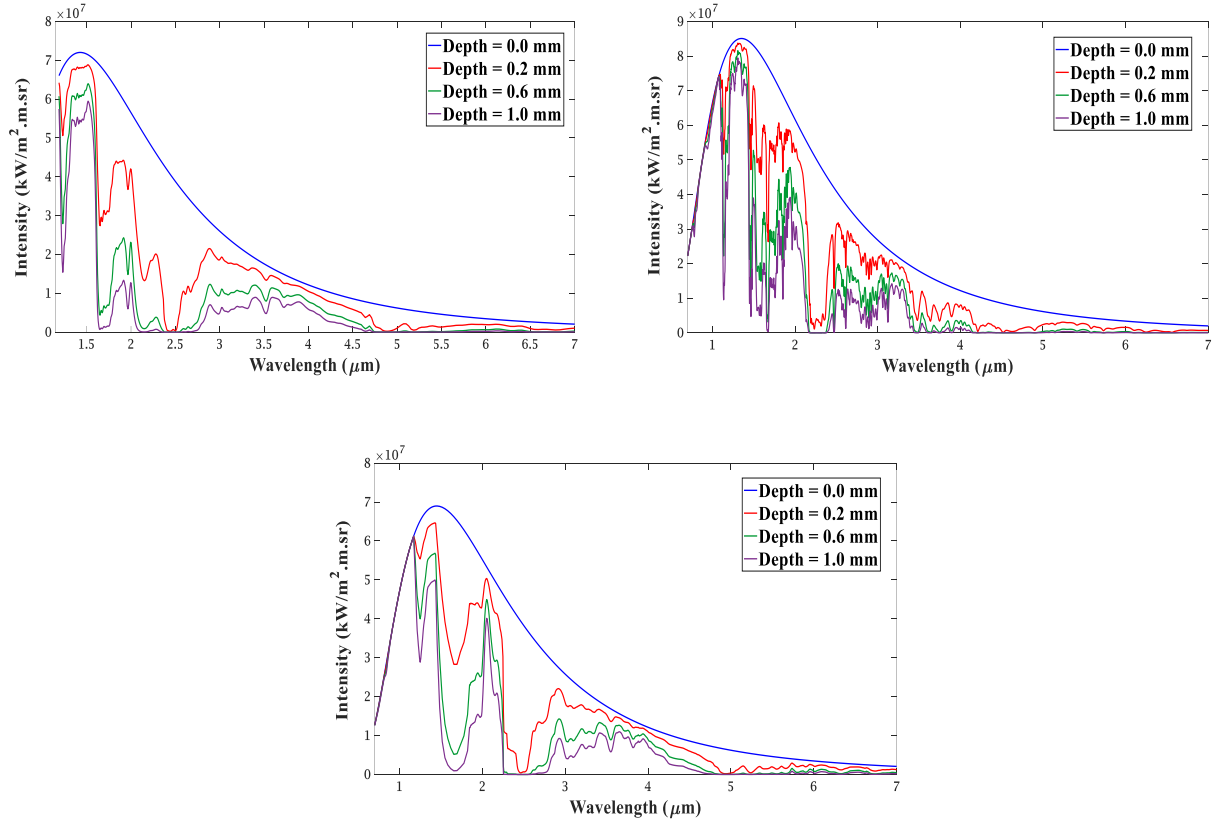409   Table 5.

410

411

412

Figure 12- The calculated spectral intensity at different depths for: left) decane right) toluene and bottom) heptane.

Although increasing the number of quadrature points in FSCK model leads to an excellent agreement with results of high-resolution method, it dismisses the main advantage of using the FSCK method which is its low computational time. Therefore, we looked for the optimal number of quadrature points which provides good accuracy for considered liquid fuels. Performing simulation for different number of quadrature points showed that with having 7 QP in FSCK model, a reasonable accuracy in radiation heat transfer simulation is achieved. As seen in Figure 13, increasing the number of quadrature points for higher than 7 does not show sensible improvement to the results while increases the time of computation.

426
427
Table 5 – Average relative error of transmissivity and radiative heat source for different radiation methods with cases with various liquid fuels.

Fuel	Solution method	Average relative error (%) for transmissivity			Average relative error (%) for radiative heat source		
		Case 1	Case 2	Case 3	Case 1	Case 2	Case 3
Decane	FSCK with 32 QP	1.47	2.02	2.06	0.44	1.01	1.38
	FSCK with 7 QP	3.93	3.29	2.91	5.35	4.82	4.21
	Gray	93.52	90.62	89.04	95.08	94.64	94.65
	Gray (T_{BC})*	93.98	91.19	89.62	96.45	96.22	96.15
Ethanol	FSCK with 32 QP	3.09	3.08	3.07	1.00	1.00	1.01
	FSCK with 7 QP	46.60	46.30	46.16	14.04	14.03	14.04
	Gray	94.66	93.95	93.59	96.59	96.62	96.61
	Gray (T_{BC})*	94.65	93.91	93.55	96.52	96.48	96.46
Ethylene Glycol	FSCK with 32 QP	14.89	12.30	10.94	5.69	5.56	5.42
	FSCK with 7 QP	38.50	31.62	27.88	31.50	30.74	29.56
	Gray	77.22	64.35	57.47	94.68	93.21	91.76
	Gray (T_{BC})*	77.15	64.30	57.42	94.39	93.00	91.55
Heptane	FSCK with 32 QP	2.51	2.50	2.49	1.09	1.07	1.05
	FSCK with 7 QP	19.75	19.66	19.60	9.46	9.42	9.39
	Gray	94.60	94.50	94.32	93.18	93.81	93.83
	Gray (T_{BC})*	95.62	95.25	95.05	96.07	95.98	95.94
Toluene	FSCK with 32 QP	0.22	0.21	0.21	0.46	0.47	0.46
	FSCK with 7 QP	5.62	5.57	5.54	2.96	2.97	2.96
	Gray	96.31	95.75	95.45	98.99	98.44	98.43
	Gray (T_{BC})*	94.71	94.22	93.93	94.28	94.27	94.36

* Gray calculations based on using Planck mean absorption coefficient of an equivalent temperature of the boundary incident radiation (i.e. 1450 K).
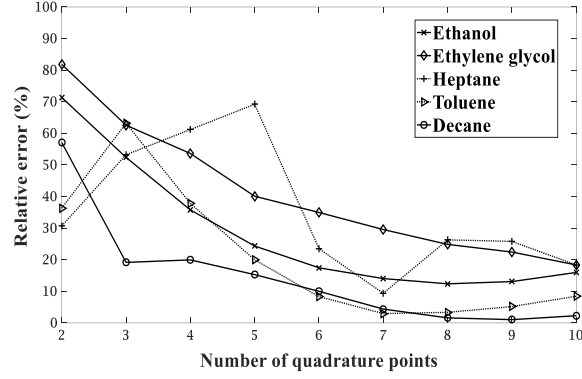
428

429

Figure 13- Relative error of calculated radiative heat source for different number of quadrature points

431   In Figure 13, the relative error is defined as:

$$relative\ error(\%) = \frac{|(\dot{q}_{rad}''')_{LBL} - (\dot{q}_{rad}''')_{FSCK}|}{(\dot{q}_{rad}''')_{LBL}} \times 100 \qquad (28)$$

432   Detail values of mean relative errors in simulation of transmissivity and heat source within the five

433   liquid fuels for different methods are summarized in Table 5. According to the presented results,

434   considering the equivalent temperature of the incident intensity does not have a substantial effect

435   on the accuracy of the gray calculations.

436   To exhibit the computational gain brought by the present FSCK model, the computational

437   time of the FSCK calculation is compared with that of the high-resolution integration method.

438   Both calculations are done on a same computer (Intel core i7 6500U processor) utilizing MATLAB

439   codes with a fairly similar programing logic. The numerical tests, showed that the computational

440   time of solving RTE by two options depends to the number of spectral divisions in high resolution

441   calculations and number of quadrature points used in FSCK model. The computational time for

442   the presented results was 0.3281 and 0.0522 s for high-resolution spectral calculations with 600

443   wavelength bands and FSCK with 7 QP respectively. About 40% of reported computational time

444   for FSCK method is due to the loading of look up tables and 25% of CPU time is consumed by

445   doing two interpolations and only 10% of computational time is devoted to solving RTE in FSCK

446   method exhibiting a remarkable computational gain of the present approach as loading of the look

447   up tables and obtaining the FSCK model data for a selected number of QP need to be done only

448   once. Hence, the actual computational gain in real applications will depend on the details of the

449   program implementation and coupling with other conservation equations.

25

450   In all the presented simulations till now, the high value of incident intensity in the upper

451   boundary made the effect of emission of the liquid negligible. Even with omitting emission term

452   from the RTE, small changes are seen in the results in which in in-line with observations in [30,

453   21]. Hence, when the incoming radiation to the boundary is strong and the liquid is relatively at

454   low temperature, assuming negligible emission is valid. However, for the situations in which the

455   boundary incident intensity is not that strong, for instance when there is radiation blockage due to

456   large amount of soot within combustion products or high deposition of soot on liquid surface, the

457   role of liquid emission becomes significant. In some cases, the intensity due to emission of the

458   liquid and incident intensity can be assumed to be in the same order of magnitude. To include this

459   kind of conditions in our investigation, a series of test cases have been performed using different

460   radiation intensity at the upper boundary. In these cases, i.e. case 4 to case 6, the radiation intensity

461   at the upper boundary is assumed to be represented by an equivalent Planck intensity of 1450 K

462   with the boundary properties given in Table 4.

463   The calculated results for different methods for these cases are shown in the following figures.

464   Due to the high discrepancy of the results for gray method for these cases and for the sake of clarity

465   of the diagrams, the results of FSCK and high-resolution method only are included in these figures.
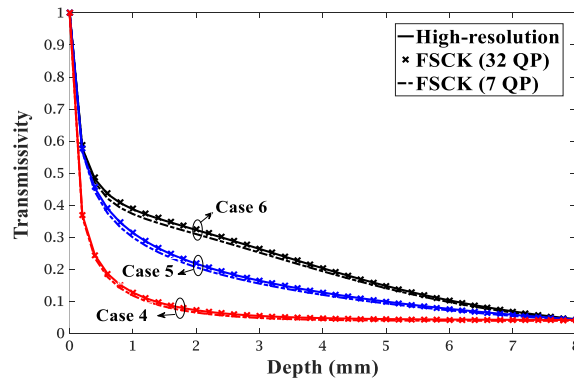

466

467   Figure 14 – The transmissivity of liquid ethylene glycol calculated by different methods for three different cases.

468   According to the calculated transmissivity shown in Figure 14, the FSCK model with 32

469   QP provides very accurate results with very low errors in comparison to high-resolution results.

470   For the case 4 (i.e. homogenous medium) it is clear that by using a large enough quadrature points

471   the results of FSCK is the same as results of high-resolution method as commonly expected from

472   FSCK model. Detailed report of relative errors for different cases has been given in Table 6.

26

473   The calculated transmissivity of liquid heptane for three cases are shown in Figure 15. For

474   heptane, the relative error for FSCK method with 32 QP is near to 1 percent. For radiative heat

475   sources, the presented results in Table 6 for mean relative errors show that using 7 QP in FSCK

476   method is sufficient to have a good accuracy.
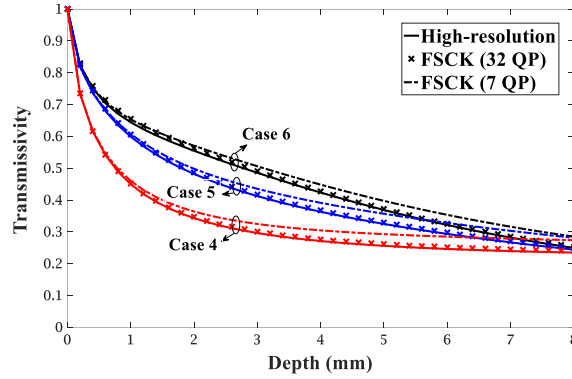

477

478   Figure 15 - The transmissivity of liquid heptane calculated by different methods for three different cases.

479   For toluene, obtained transmissivities for cases 4 to 6 has been presented in Figure 16.

480   Results for different cases show the good accuracy especially for FSCK with 7 QP. The relative

481   error in transmissivities for toluene is less than 1 percent with using of 32 QP in FSCK method. In

482   case of FSCK method with 7 QP, results show a very good agreement with high-resolution

483   calculations. Relative errors for transmissivity and radiative source terms for these three cases have

484   been reported in Table 6.
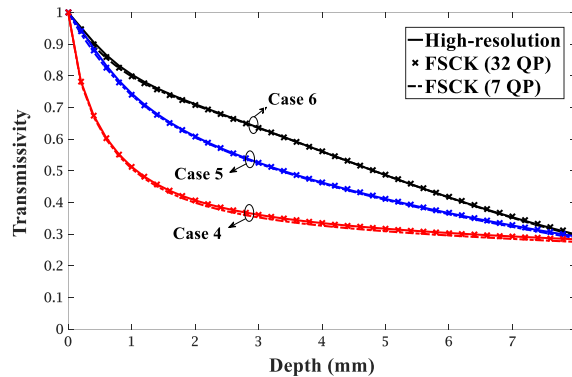

485

486   Figure 16 - The transmissivity of liquid toluene calculated by different methods for three different cases.

487   Calculated transmissivity for decane for the cases 4 to 6 has been presented in Figure 17.

488   According to results, for homogenous media, FSCK results with 32 and 7 QP show excellent

489   agreement with those of high resolution method. For case 5 and 6, error increases similar to the

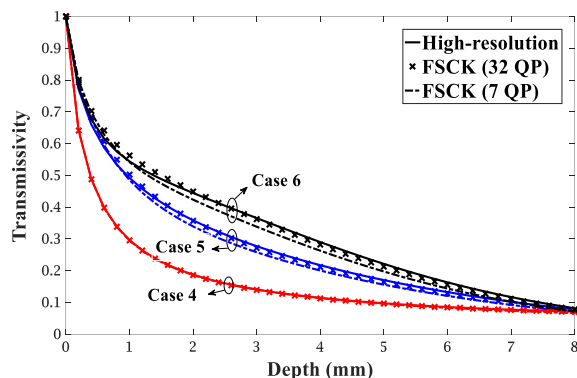490   results of other liquid fuels.

491

492   Figure 17 – The transmissivity of liquid decane calculated by different methods for three different cases.

493   Finally, the calculated transmissivities for ethanol for different cases are shown in Figure

494   18. Similar to the previous results, an excellent agreement is seen between the results of high-

495   resolution method and the FSCK method with 32 QP. This shows that for ethanol in order to have

496   very high accuracy, it is necessary to choose higher number of quadrature points compared to
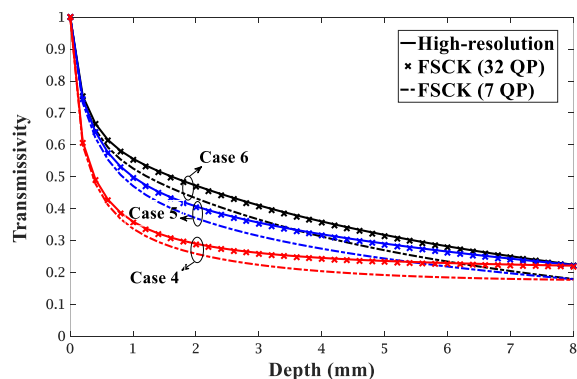
497   toluene and decane.

498

499   Figure 18 - The transmissivity of liquid ethanol calculated by different methods for three different cases.

500

501   Relative errors of the estimated transmissivities and radiative heat sources of different fuels for

502   three cases are summarized in Table 6. Presented results in this section showed that for the cases

503   in which the emission of liquid plays an important role, using FSCK method bring more advantage

504   to the calculations.

505

Table 6– Average relative error of calculated transmissivity and radiative heat source using different radiation methods for considered liquid fuels with three different cases.

Fuel	Solution method	Average relative error (%) for transmissivity			Average relative error (%) for radiative heat source		
		Case 4	Case 5	Case 6	Case 4	Case 5	Case 6
Decane	FSCK with 32 QP	0.91	2.40	3.17	0.58	7.56	14.57
	FSCK with 7 QP	1.24	6.80	8.14	3.47	9.32	21.03
	Gray	53.19	34.96	30.28	91.42	87.57	91.67
	Gray (T_{BC})*	54.72	35.57	30.92	93.79	90.37	93.87
Ethanol	FSCK with 32 QP	1.09	0.99	0.96	0.84	1.16	1.79
	FSCK with 7 QP	14.55	12.91	12.32	13.31	13.27	13.80
	Gray	30.30	23.84	21.86	94.59	94.13	94.38
	Gray (T_{BC})*	30.29	23.82	21.84	94.43	93.87	94.10
Ethylene glycol	FSCK with 32 QP	1.28	0.82	0.80	5.15	3.76	5.23
	FSCK with 7 QP	8.47	5.18	4.45	29.26	21.48	17.00
	Gray	25.93	11.45	9.14	92.89	75.04	78.78
	Gray (T_{BC})*	25.87	11.41	9.09	92.21	74.39	78.34
Heptane	FSCK with 32 QP	1.58	1.23	1.08	1.01	1.88	3.88
	FSCK with 7 QP	10.53	7.57	6.38	8.60	8.45	8.18
	Gray	61.15	49.09	44.67	87.21	86.86	90.98
	Gray (T_{BC})*	61.94	49.73	45.31	92.59	91.60	94.86
Toluene	FSCK with 32 QP	0.10	0.27	0.37	0.50	2.27	3.75
	FSCK with 7 QP	2.13	0.87	0.41	3.40	5.39	8.12
	Gray	56.43	43.48	38.74	97.74	114.60	115.58
	Gray (T_{BC})*	55.27	42.35	37.58	88.48	101.05	107.02

* Gray calculations based on using Planck mean absorption coefficient of an equivalent temperature of the boundary incident radiation (i.e. 1450 K).

508

509 As explained in the theory section, choosing reference temperature has influence on
510 accuracy of the FSCK model. All of the explanations about the reference temperature in the

511 literature was for the gas phase where temperature of medium is generally higher than in condensed

512 phase. For liquid, the situation is different from gas phase because its temperature varies between

513 room temperature and boiling temperature of the liquid and the maximum temperature, i.e.

514 boundary temperature, is coming from out of the computational domain. To investigate the effect

515 of reference temperature on the accuracy of the FSCK model, FSCK model is applied to the

516 heptane pool using three different reference temperatures. Using linear temperature profile for the

517 medium, i.e. case 2, the volume average and Planck-mean reference temperature are obtained as

518 351.99 and 337.15 K, respectively. The third choice for reference temperature is the temperature

519 of the upper boundary which represent the radiation feedback to the pool. It is assumed to be 1450

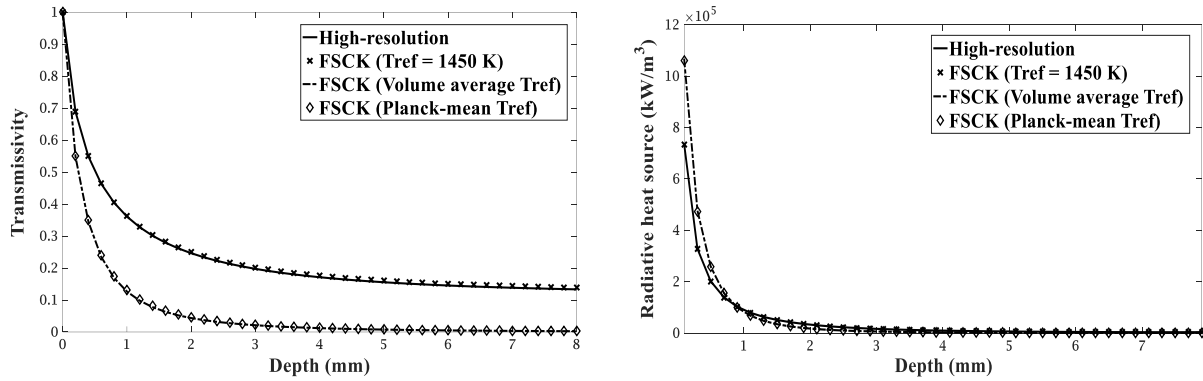520 K as suggested in [41]. Results of these three choices are shown in Figure 19.

521 Figure 19 – Comparison of the transmissivity (left plot) and radiative heat source (right plot) for different reference
522 temperatures.

523 Figure 19 shows that using volume average and Planck-mean temperature as the reference

524 temperature in FSCK calculations leads to poor accuracy while using the upper wall temperature

525 provides very good agreement with the high-resolution reference solution. One can conclude that

526 the equivalent temperature representing the radiation reaching the interface of the liquid phase

527 should be used as the reference temperature in FSCK calculations within the liquid phase. With

528 the selection of upper wall temperature as reference temperature, the absorption coefficient in the

529 FSCK equation is calculated using the spectral information corresponded to the incident intensity

530 at boundary that is the most important in absorption within the liquid domain. In simulations of

531 radiation transfer for combustion applications, the incident intensity that reaches from the flame

532 region to the liquid surface must be treated accurately within the domain. Therefore, in contrary to

533 the gas phase FSCK calculations, using upper wall temperature or equivalent temperature for the

30

534   incident intensity at the interface of the liquid layer should be used as the reference temperature to

535   guarantee a good accuracy.

536   This importance of incident intensity at the liquid interface is not due to the larger value of

537   the reaching integrated radiation flux to the fuel surface in comparison to the emission of liquid,

538   but it is because of the spectral profile of the incoming radiation. To exemplify this claim, the next

539   simulation has been done with 1 percent of incident intensity at the upper wall. With doing this

540   modification, the emission of the liquid fuel will be in the same order of magnitude with incident

541   intensity at the boundary. In this case also, the results shown in Figure 20 exhibit better accuracy

542   for the case of choosing the upper wall temperature as the reference state.
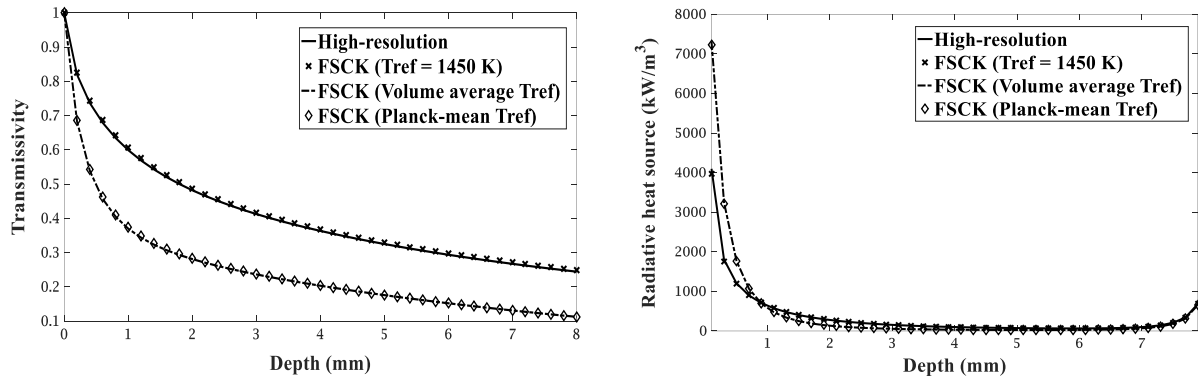

543   Figure 20 - Comparison of the transmissivity (left plot) and radiative heat source (right plot) for different reference
544   temperatures with lower incident radiation at the boundary

545   As a conclusion to results in Figure 19 and Figure 20, in simulation of radiation transfer

546   within liquids, selecting an equivalent temperature of the incident intensity reaching the liquid

547   interface is recommended to ensure high accuracy of FSCK method. The same simulations have

548   been done using temperature of 700 K for upper wall. In this case, the spectral profile of the

549   incoming radiation and specially its peak region has a better similarity to the Planck distribution

550   at liquid temperature, so their k-distribution is better correlated with each other. Therefore, the

551   selection of reference temperature does not cause that much difference.

552   It is worth mentioning that the present article aims at development of FSCK model and its

553   parameters in the form of look up tables for liquid fuels. However, in many practical conditions

554   especially in gas-droplet flows where gas radiation is mainly dominant and the droplets only

555   occupy a small fraction of the space, the spectral radiation should be solved in an integral manner

556   for the gas and liquid phase. It is not easy to develop such a model as shown in the recent work of

31

557 Wang and coworkers [13] who introduced the FSK-FSK method to solve spectral radiation for gas
558 and solid flow. In their work, difference between the particles temperature and gas medium was
559 the main barrier to obtain an accurate k-distribution for both phases. However, in the present
560 research our main application was liquid pool fires where the gas and liquid phases are clearly
561 separated and therefore can be solved as two separate systems leading to two separate RTE solvers
562 connected through an appropriate boundary condition at the liquid interface. We are currently work
563 on development of integrated version of FSCK for both liquid and gas which will be presented in
564 our next papers.

4.1. Generating look up tables for liquid fuels

566   Choosing temperature of upper wall as reference temperature makes the size of the data for
567 the FSCK model smaller. The most effective way to facilitate using FSCK method is to generate
568 look-up table for a range of possible thermal conditions. For the five fuels studied in the paper, a
569 specified number of temperature steps is considered to cover the range of possible local
570 temperatures of the liquid (T) from the room temperature 300 K to the boiling temperature of each
571 fuel with step of 10 K that facilitates the implementation of the model to account for small
572 temperature change within the fuels. To generalize the look-up table data for different applications,
573 the range of source temperature, T_{ref}, (i.e. the reference temperature as well) has been chosen from
574 300 K to 2000 K by step of 50 K. The look up table includes the data of $a(T, T_{ref}, g_{ref})$ and
575 $k(T_{ref}, g_{ref})$ as explained in section 2.2. Data of the look-up tables has been presented for 32 QP.
576 The FSCK model parameters for lower number of QP can be attained by interpolation through the
577 provided data of 32 QP.

5. Conclusions

579   In this research, the FSCK models were developed for the simulation of radiation transfer
580 within five different hydrocarbon liquid fuels. The developed models were validated for several
581 different thermal conditions in liquid pool fires. The benchmark solutions were first obtained by
582 solving the spectral RTE using the high resolution spectral data taken from literature, and then
583 used to assess the accuracy of the developed FSCK models, exploring the effects of model
584 parameters such as the number of quadrature points (QP) and the reference temperature (T_{ref}) .

585   Simulation results showed that for many fuels, 7 QP can be an optimal option for the FSCK

586   calculations to provide a good accuracy with a reasonable computational cost. Strong absorption

587   within the liquid makes the shape of spectral intensity to deviate from the shape of intensity at

588   boundary. This deviation decreases the accuracy of calculated k-distribution with applying

589   boundary temperature as reference state especially for ethylene glycol that has the highest error in

590   results.

591   However, in general the proposed FSCK method provided much more accurate results for the

592   transmissivity and heat source than the gray method. Moreover, compared to the high resolution

593   calculations, the present FSCK model is much faster with fairly small loss of accuracy.

594   The role of the reference temperature was studied using three different options, i.e. volume

595   averaged temperature, Planck-mean temperature, and the equivalent temperature of incident

596   intensity. The results showed that for the liquid fuels, using an equivalent temperature of incident

597   intensity at the interface of the liquid layer led to the highest accuracy and is the best option when

598   applying the FSCK method for liquid heat transfer calculations.

599   To facilitate the implementations of the developed model, we provide a comprehensive look up

600   table of the FSCK model parameters with a large number of quadrature points. The provided look

601   up table covers a wide range of thermal conditions which may occur in different application

602   including fire scenarios. For future development, simulations with FSCK method can be done with

603   more realistic flame heat feedback instead of using simplified condition of black wall.

604   **Acknowledgements**

608   **Appendix A. Supplementary material**

609   Supplementary data associated with this article is an excel file including all the look up table data

610   obtained for different fuels at various reference and local temperatures with 32 QPs and a short

611   description of the data. The supplementary material can be found in the online version, at ….

612

613 **References**

614

[1] M. H. Bordbar and T. Hyppänen, "Multiscale Numerical Simulation of Radiation Heat Transfer in Participating Media," *Heat Transfer Engineering,* vol. 34, pp. 54-69, 2013.

[2] M. H. Bordbar and T. Hyppänen, "The correlation based zonal method and its application to the back pass channel of oxy/air-fired CFB boiler," *Applied Thermal Engineering,* vol. 78, pp. 351-363, 2015.

[3] G. C. Fraga, H. Bordbar, S. Hostikka and F. H. R. França, "Benchmark Solutions of Three-Dimensional Radiative Transfer in Nongray Media Using Line-by-Line Integration," *Journal of Heat Transfer,* vol. 142, 2020.

[4] H. Bordbar and S. Hostikka, "Numerical Solution of LBL Spectral Radiation of a Heptane Pool Fire," in *the 9th International Symposium on Radiative Transfer, RAD-19*, Athens, Greece,, 2019.

[5] H. Bordbar, S. Hostikka, G. Parent and P. Boulet, "Numerically Resolved Line by Line Radiation Spectrum of Large Kerosene Pool," *Journal of Quantitative Spectroscopy and Radiative Transfer,* p. Submitted, 2020.

[6] H. Bordbar, A. Maximov and T. Hyppänen, "Improved banded method for spectral thermal radiation in participating media with spectrally dependent wall emittance," *Applied energy,* vol. 235, pp. 1090-1105, 2019.

[7] H. Bordbar and T. Hyppänen, "Line by line based band identification for non-gray gas modeling with a banded approach," *Int. J. Heat Mass Transf.,* vol. 127, pp. 870-884, 2018.

[8] H. Bordbar, G. C. Fraga and S. Hostikka, "An extended weighted-sum-of-gray-gases model to account for all CO_2 - H_2O molar fraction ratios in thermal radiation," *International Communications in Heat and Mass Transfer,* vol. 110, p. 104400, 2020.

[9] M. H. Bordbar, G. Wecel and T. Hyppänen, "A line by line based weighted sum of gray gases model for inhomogeneous CO_2–H_2O mixture in oxy-fired combustion," *Combust. Flame,* vol. 161, p. 2435–2445, 2014.

[10] Y. Sun and X. Zhang, "Contributions of gray gases in SLW for non-gray radiation heat transfer and corresponding accuracies of FVM and P1 method," *International Journal of Heat and Mass Transfer,* vol. 121, pp. 819-831, 2018.

[11] V. P. Solovjov, F. Andre, D. Lemonnier and B. W. Webb, "The generalized SLW model," in *Journal of Physics: Conference Series*, 2016.

[12] M. F. Modest and H. Zhang, "The full-spectrum correlated-k distribution and its relationship to the weighted-sum-of-gray-gases method," *ASME-PUBLICATIONS-HTD,* vol. 366, pp. 75-84, 2000.

[13] C. Wang, B. He and M. F. Modest, "Full-spectrum correlated-k-distribution look-up table for radiative transfer in nonhomogeneous participating media with gas-particle mixtures," *International Journal of Heat and Mass Transfer,* vol. 137, pp. 1053-1063, 2019.

[14] M. F. Modest, "Narrow-band and full-spectrum k-distributions for radiative heat transfer—correlated-k vs. scaling approximation," *Journal of Quantitative Spectroscopy and Radiative Transfer,* vol. 76, pp. 69-83, 2003.

[15] M. F. Modest, "Chapter 20 - Solution Methods for Nongray Extinction Coefficients," in *Radiative Heat Transfer (Third Edition)*, Third Edition ed., M. F. Modest, Ed., Boston, Academic Press, 2013, pp. 626-693.

[16] M. F. Modest and H. Zhang, "The full-spectrum correlated-k distribution for thermal radiation from molecular gas-particulate mixtures," *J. Heat Transfer,* vol. 124, pp. 30-38, 2001.

[17] S. Mazumder and M. F. Modest, "Application of the full spectrum correlated-k distribution approach to modeling non-gray radiation in combustion gases," *Combustion and Flame,* vol. 129, pp. 416-438, 2002.

[18] C. Wang, W. Ge, M. F. Modest and B. He, "A full-spectrum k-distribution look-up table for radiative transfer in nonhomogeneous gaseous media," *Journal of Quantitative Spectroscopy and Radiative Transfer,* vol. 168, pp. 46-56, 2016.

[19] C. Wang, M. F. Modest and B. He, "Full-spectrum correlated-k-distribution look-up table for use with radiative Monte Carlo solvers," *International Journal of Heat and Mass Transfer,* vol. 131, pp. 167-175, 2019.

[20] C. Ates, N. Selçuk and G. Kulah, "Influence of gray particle assumption on the predictive accuracy of gas property approximations," *Journal of Quantitative Spectroscopy and Radiative Transfer,* vol. 220, pp. 67-83, 2018.

[21] T. Isojärvi, H. Bordbar and S. Hostikka, "Calculation of radiation transmittance through n-heptane in a pool fire," in *Journal of Physics: Conference Series*, 2018.

[22] C. Ates, G. Ozen, N. Selçuk and G. Kulah, "Radiative heat transfer in strongly forward scattering media of circulating fluidized bed combustors," *Journal of Quantitative Spectroscopy and Radiative Transfer,* vol. 182, pp. 264-276, 2016.

[23] M. H. Bordbar, K. Myöhänen and T. Hyppänen, "Coupling of a radiative heat transfer model and a three-dimensional combustion model for a circulating fluidized bed furnace," *Applied Thermal Engineering,* vol. 76, pp. 344-356, 2015.

[24] A. Hamins, S. J. Fischer, T. Kashiwagi, M. E. Klassen and J. P. Gore, "Heat Feedback to the Fuel Surface in Pool Fires," *Combustion Science and Technology,* vol. 97, pp. 37-62, 1994.

[25] J. G. Quintiere, "Surface flame spread," *SFPE handbook of fire protection engineering,* vol. 2, 2002.

[26] S. C. Kim, K. Y. Lee and A. Hamins, "Energy balance in medium-scale methanol, ethanol, and acetone pool fires," *Fire Safety Journal,* 2019.

[27] J. Zhao, H. Huang, H. Wang, J. Zhao, Q. Liu and Y. Li, "Experimental study on burning behaviors and thermal radiative penetration of thin-layer burning," *Journal of Thermal Analysis and Calorimetry,* vol. 130, pp. 1153-1162, 2017.

[28] J. Zhao, H. Huang, G. Jomaas, M. Zhong and R. Yang, "Experimental study of the burning behaviors of thin-layer pool fires," *Combustion and Flame,* vol. 193, pp. 327-334, 2018.

[29] T. Sikanen and S. Hostikka, "Modeling and simulation of liquid pool fires with in-depth radiation absorption and heat transfer," *Fire Safety Journal,* vol. 80, pp. 95-109, 2016.

[30] T. Isojärvi, H. Bordbar and S. Hostikka, "Spectrally resolved calculation of thermal radiation penetration into liquid n-heptane in pool fires," *International Journal of Heat and Mass Transfer,* vol. 127, pp. 1101-1109, 2018.

[31] J. R. Howell, M. P. Menguc and R. Siegel, Thermal radiation heat transfer, CRC press, 2015.

[32] C. C. Wang, J. Y. Tan, C. Y. Jing and L. H. Liu, "Temperature-dependent optical constants of liquid isopropanol, n-butanol, and n-decane," *Applied optics,* vol. 57, pp. 3003-3011, 2018.

[33] Q. Ai, M. Liu, F. Sun, C. Liu and X. Xia, "Near infrared spectral radiation properties of different liquid hydrocarbon fuels," *Journal of Near Infrared Spectroscopy,* vol. 26, pp. 5-15, 2018.

[34] A. Bansal, M. Modest and D. Levin, "Correlated-k Distribution Method for Atomic Radiation in Hypersonic Nonequilibirum Flows," in *47th AIAA Aerospace Sciences Meeting including The New Horizons Forum and Aerospace Exposition*, 2009.

[35] A. Bansal, M. F. Modest and D. A. Levin, "Multi-scale k-distribution model for gas mixtures in hypersonic nonequilibrium flows," *Journal of Quantitative Spectroscopy and Radiative Transfer,* vol. 112, pp. 1213-1221, 2011.

[36] J. Cai and M. F. Modest, "Improved full-spectrum k-distribution implementation for inhomogeneous media using a narrow-band database," *Journal of Quantitative Spectroscopy and Radiative Transfer,* vol. 141, pp. 65-72, 2014.

[37] A. Wang, "High-accuracy, compact database of narrow-band k-distributions for water vapor and carbon dioxide," in *ICHMT DIGITAL LIBRARY ONLINE*, 2004.

[38] E. Sani and A. Dell'Oro, "Spectral optical constants of ethanol and isopropanol from ultraviolet to far infrared," *Optical Materials,* vol. 60, pp. 137-141, 2016.

[39] E. Sani and A. Dell'Oro, "Optical constants of ethylene glycol over an extremely wide spectral range," *Optical Materials,* vol. 37, pp. 36-41, 2014.

[40] J. J. Kelly, C. H. Barlow, T. M. Jinguji and J. B. Callis, "Prediction of gasoline octane numbers from near-infrared spectral features in the range 660-1215 nm," *Analytical Chemistry,* vol. 61, pp. 313-320, 1989.

[41] J. M. Suo-Anttila, T. K. Blanchat, A. J. Ricks and A. L. Brown, "Characterization of thermal radiation spectra in 2 m pool fires," *Proceedings of the Combustion Institute,* vol. 32, pp. 2567-2574, 2009.

[42] M. R. Anderson, "Determination of infrared optical constants for single component hydrocarbon fuels," 2000.

[43] S. Kedenburg, M. Vieweg, T. Gissibl and H. Giessen, "Linear refractive index and absorption measurements of nonlinear optical liquids in the visible and near-infrared spectral region," *Optical Materials Express,* vol. 2, pp. 1588-1611, 2012.

[44] J. E. Bertie, R. N. Jones, Y. Apelblat and C. D. Keefe, "Infrared intensities of liquids XIII: Accurate optical constants and molar absorption coefficients between 6500 and 435 cm-1 of toluene at 25° C, from spectra recorded in several laboratories," *Applied spectroscopy,* vol. 48, pp. 127-143, 1994.

[45] M. F. Modest, "Chapter 1 - Fundamentals of Thermal Radiation," in *Radiative Heat Transfer (Third Edition)*, Third Edition ed., M. F. Modest, Ed., Boston, Academic Press, 2013, pp. 1-30.

[46] A. Vali, D. S. Nobes and L. W. Kostiuk, "Fluid motion and energy transfer within burning liquid fuel pools of various thicknesses," *Combustion and Flame,* vol. 162, pp. 1477-1488, 2015.

[47] A. Vali, D. S. Nobes and L. W. Kostiuk, "Transport phenomena within the liquid phase of a laboratory-scale circular methanol pool fire," *Combustion and flame,* vol. 161, pp. 1076-1084, 2014.

615

616